Physical Model of the Dynamic Instability in an Expanding Cell Culture

Shirley Mark,[†] Roie Shlomovitz,[†] Nir S. Gov,[†*] Mathieu Poujade,[‡] Erwan Grasland-Mongrain,[‡] and Pascal Silberzan[‡]

[†]Department of Chemical Physics, The Weizmann Institute of Science, Rehovot, Israel; and [‡]Laboratoire Physico-Chimie Curie, UMR 168, Institut Curie, Centre de Recherche, Centre National de la Recherche Scientifique, Université Pierre et Marie Curie, Paris, France

ABSTRACT Collective cell migration is of great significance in many biological processes. The goal of this work is to give a physical model for the dynamics of cell migration during the wound healing response. Experiments demonstrate that an initially uniform cell-culture monolayer expands in a nonuniform manner, developing fingerlike shapes. These fingerlike shapes of the cell culture front are composed of columns of cells that move collectively. We propose a physical model to explain this phenomenon, based on the notion of dynamic instability. In this model, we treat the first layers of cells at the front of the moving cell culture as a continuous one-dimensional membrane (contour), with the usual elasticity of a membrane: curvature and surface-tension. This membrane is active, due to the forces of cellular motility of the cells, and we propose that this motility is related to the local curvature of the culture interface; larger convex curvature correlates with a stronger cellular motility force. This shape-force relation gives rise to a dynamic instability, which we then compare to the patterns observed in the wound healing experiments.

INTRODUCTION

Cell motility plays a key role in the functioning of multicellular organisms (1). It is now clear that the key components in this process are the internal forces created by the cytoskeleton (mainly actin, myosin, and adhesion molecules), and involves specialized subcellular structures such as lamellipodia and filopodia (2). When cells are part of a culture, or tissue, they normally have strong cell-cell contacts, so that the culture is continuous. In such cases, motility of individual cells translates into collective motion of all the cells in the culture (3–5). Furthermore, it was observed that the cells at the outer rim of a two-dimensional cell culture are the most motile (6). This phenomenon of collective cellular motions is observed in wound healing model experiments (3–5) and in morphogenesis and embryogenesis (7). Cells inside cultures can move in a random-walk-like fashion or can show a directional motility that is often controlled by external directional signals, such as chemotaxis due to a chemical gradient (8,9).

Recent experiments (3) on wound healing models have found conditions where the expanding contour of the cell culture develops fingering patterns. In these experiments, there is no cell injury or growth factors that trigger the cell motility (10), which is therefore triggered simply by the sudden release of the confinement placed at the boundaries of the cell culture (4). After the release of the confinement, the cells migrate onto the surrounding free substrate in columns (i.e., fingers), where the tips of these fingers contain leader cells that have a very different morphology; they are highly polarized and motile with a large crescent-shaped and highly developed lamellipodia. Proposing a physical mechanism that serves to drive the formation of these fingering patterns (11) is the main purpose of this article.

Previous modeling of this system was based on the chemical signaling between cells (12–14), which is triggered at the wound location when cells are either injured or simply have the confinement released (4). This chemical signaling (15), which emanates from the cells at the culture edge and then propagates and diffuses into the culture itself, triggers cellular motility toward the free substrate (wound). When there is no cell injury, and a weaker chemical signal is present, the collective motion was observed to be much slower on average. Previous models also included the contact inhibition of cells, whereby cells tend to migrate toward regions of lower cell density (16), and proliferate there (17), as well as mechanical contact with the substrate. There are other models that describe the closure of the wound as a result of single cell dynamics (18,19). A recent model of this kind was shown to also give rise to fingering growth (20).

We propose here a new model that is based on a direct relation between the shape of the cells and their motility, in which we neglect any effects of chemical signaling. Such a model has not been previously explored (to our knowledge), and we demonstrate here that it can provide a mechanism for the formation of patterns in expanding cell cultures. We find that our model gives rise to a surface instability and the spontaneous formation of growing fingers, as observed in the experiments (3). Note that our model applies to the first stages of the wound-healing process, and does not describe the large-scale coalescence of the tissues when the wound closes.

THE MODEL

As we described above, the leader cells at the tips of the migrating columns of cells have the most highly developed

Submitted July 30, 2009, and accepted for publication October 15, 2009.

*Correspondence: nirgov@weizmann.ac.il or nirgov@wisemail.weizmann.ac.il

Editor: Alexander Mogilner.

0006-3495/10/02/0361/10 $2.00

doi: 10.1016/j.bpj.2009.10.022

motility machinery, i.e., a large lamellipodia and many adhesion contacts. Together, these features provide the leader cells with the ability to produce a strong traction force (21) that pulls and directs the motion of the cells behind it. Although cells deeper within the culture also contribute a nonvanishing traction (2), the cells in the first ~5–10 cell layers seem to be dominant in determining the overall migration of the cell culture (6). (Note that organized cellular flows behind the leader cells can extend to several cell layers; L. Petitjean, M. Reffay, E. Grasland-Mongrain, M. Poujade, B. Ladoux, A. Buguin, and P. Silberzan, unpublished.) This assumption is reinforced by force-mapping experiments on cellular cultures, which show that the forces generated by the cells at the edge are stronger than the forces applied to the substrate by the rest of the culture (6,23). We note that the leader cells have a relatively high convex shape. The relation between cell shape and the activation of the internal motility machinery was observed in a number of examples, at the single cell level:

1. Cells grown on adhesive micropatterns exhibit membrane protrusive activity at the most highly curved parts of the cells (24), where traction forces are concentrated (25).
2. Discoid cellular fragments become motile after an applied mechanical stimulus that changed them into a crescent shape (26).
3. Releasing cells from shaped confinement is enough to trigger directional cell movement (27).

We are therefore motivated by these observations to suggest that there is a positive feedback between the overall shape of the cell and its ability to produce motility. The motility of the leader cells in the culture interface is therefore determined by their local shape, which is imposed by their interactions with the neighboring cells. Specifically, a highly curved (crescent) cellular shape correlates with higher cellular motility. An increased motility with increasing convex curvature of the cells at the culture edge may also be triggered by the longer cell-free edge in these cells. The longer cell-free edge means that membrane receptors are more exposed to external signals, such as growth-factor receptors (10) that trigger motility. The lower number of cell-cell contacts in these cells translates into lower contact-inhibition of motility (4).

The phenomena of unstable surface growth is found in a variety of physical processes (28,29), such as crystal growth and cellular cultures (30), and many physical models have been proposed to describe these diverse phenomena (31–34). Similarly, our model includes a force that drives the instability and growth, which in our case originates from the internal motility of the cells, and is taken to be proportional to the local contour geometry. The positive feedback between the contour shape and the cell motility (driving force) gives rise to a dynamic instability. In addition there are elastic restoring forces that oppose the shape deformation, and lead to a tip-splitting phenomenon. The restoring forces arise from the elasticity of the cells, as discussed below.

As the cells maintain their contacts with their neighbors at all times, i.e., no gaps appear in the expanding culture or in its moving front, we will propose a simple model that maps this interface to a continuous one-dimensional active membrane (contour), whereas the cells in the bulk of the culture behind the front are treated as a viscous fluid (Fig. 1*a*). The sum of the internal forces, which are due to the motility of the cells at the outer layers of the culture (9), provide the driving force that moves the cells and the interface outwards in the normal direction. Counteracting these driving forces are restoring forces arising from the effective friction of the cells with the substrate, and the effective surface tension and curvature bending modulus of the cells at the culture interface. The effective bending modulus of the outer few layers of cells arises from the membrane elasticity of the individual cells, as well as from cell-cell adhesion contacts mediated by cadherin-based junctions, which connect the cytoskeleton of the individual cells into a multicellular continuous actin belt (3,35). The effective surface tension of the first few layers of cells arises from the same cell-cell interactions, and the elasticity of the individual cells. Note that the value of the effective surface tension of the outer contour can be quite low due to the ability of cells to relieve the elastic stresses by leaving or joining the edge layers from the bulk of the culture, and by reorganizing their cytoskeleton to accommodate large shape changes. These processes mean that our contour itself stretches in a viscoelastic manner, which is here approximated as purely elastic, but with a reduced stretching modulus.

In addition to the cell motility there is cell proliferation that may contribute to the expansion of the cell culture. In the recent experiments (3), it was found that during the first stages of the culture expansion (up to 15 h) there was no strong effect of the cell proliferation on the rate of culture expansion. This observation indicates that in these systems, cell motility dominates the early stages of the culture expansion. For simplicity we therefore neglect here any positive contribution of cell proliferation to the expansion of the culture, although this can be easily added to the model. Nevertheless, when the culture area expands faster than the rate of proliferation, it means that the area per cell increases. When this parameter increases beyond some threshold, we expect that there will be an elasticlike restoring force from cell stretching, which opposes the growth of the culture area.

The mathematical description of the model

The culture interface is modeled here as a one-dimensional membrane (contour), described by a Helfrich energy functional (36), which has bending and surface tension terms

$$F = W \int^{S_t} \left(\frac{1}{2}\kappa H^2 + \gamma \right) ds, \qquad (1)$$

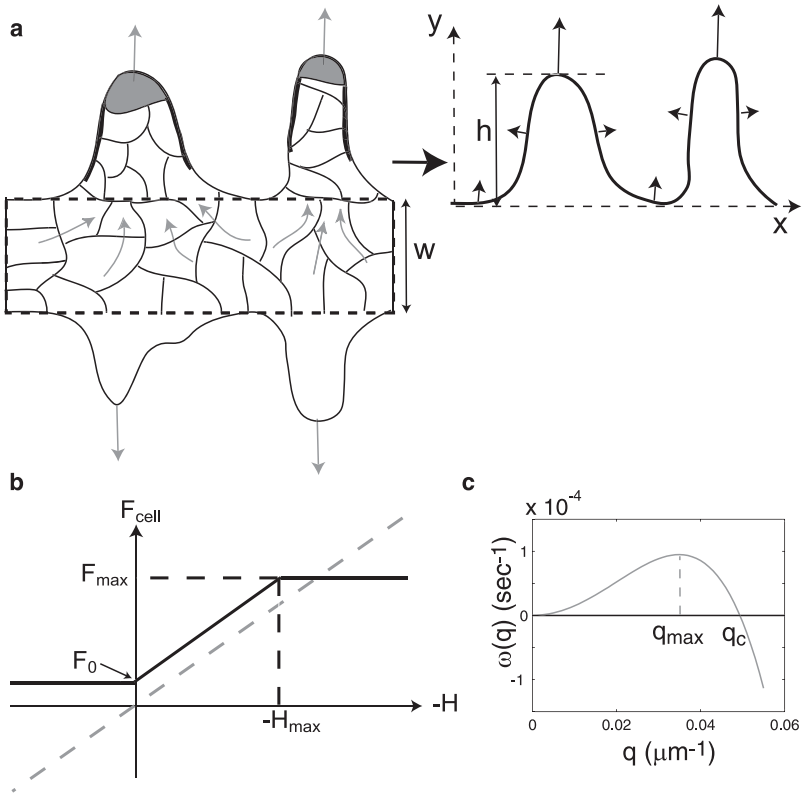

FIGURE 1 (*a*) Schematic representation of the mapping of the expanding rectangular culture (*left*), of initial width w, where the local cell motility is indicated by the shaded arrows. The leader cells are indicated by shading at the tips of the columns of cells (i.e., fingers) (11). This system is mapped in the model to a dynamic contour in the x,y plane, where the local velocity (*solid arrows*) depends on the local shape (curvature). The height of the fingers h is given by the maximal y coordinate. (*b*) The force-curvature rule that was used to describe the shape-dependence of the cell motility, as given in Eq. 4. The linear approximation used in the linear-stability analysis is indicated by the dashed line (Eq. 8). (*c*) A typical dispersion curve $\omega(q)$ for the linearized model, indicating the unstable mode $q < q_c$ and the most unstable model q_{max}.

where γ is the effective surface tension, κ is the effective curvature modulus of the culture interface, $H = \vec{H}\cdot\hat{n}$ is the size of the local membrane curvature $\vec{H} = \partial^2\vec{r}/\partial s^2$ (where $\hat{n}$ is the outward unit normal along the contour), s is the contour arc-length, and S_t is the total length of the interface (which changes with time). The thickness of the cell layer is $W \sim 3$–5 μm. Variation of this free energy with respect to $\vec{r}(s)$ gives the restoring forces per unit length, acting on each element of the interface (details are given in the Supporting Material):

$$-\frac{\delta F}{\delta \vec{r}} = W\left(-\kappa\frac{\partial^2\vec{H}}{\partial s^2} + \gamma\vec{H} - \frac{3}{2}\kappa\vec{H}^3\right). \quad (2)$$

We now add the forces produced by the cells:

1. The internal force due to the cellular motility, pushing the interface normally outwards F_{cell}.
2. The normal restoring force due to bulk cell density F_ρ (where the average cell density is $\rho = N_{cell}/Area$).
3. A noise term ν due to the random velocity of the cells.

Furthermore, although we assume that the bulk of the cell culture behind the front behaves as a viscous fluid (34), we neglect long-range hydrodynamiclike interactions through this cellular medium. This is a simplifying assumption, and renders the treatment of the model into a local form. Future treatment of the bulk culture behind the front will have to include the fact that all the cells produce local active forces, and have elastic responses (6,17).

Altogether we get the following equation of motion for the interface

$$\frac{d\vec{r}}{dt} = -\frac{\kappa}{\eta}\frac{\partial^2\vec{H}}{\partial s^2} + \frac{\gamma}{\eta}\vec{H} - \frac{3\kappa}{2\eta}\vec{H}^3 + \frac{(F_{cell} + F_\rho)\hat{n}}{\eta} + \nu\hat{n}, \quad (3)$$

where η is an effective local friction coefficient (which contains the layer thickness W from Eq. 2) arising from the cell-substrate adhesion and the effective viscosity of the two-dimensional flowing film of cells.

The main proposal in our model is that the cells' motile force increases with the convex shape, as described above. For simplicity, we assume that the cellular pushing force F_{cell} increases linearly (any other monotonously increasing relation can be implemented and will not qualitatively change the behavior) with the convex curvature (negative H) of the interface, according to (Fig. 1 *b*)

$$F_{cell} = \begin{cases} F_0 & H > 0 \\ \alpha\eta|\vec{H}| & 0 > H > -H_{max} \\ F_{max} & H < -H_{max} \end{cases}, \quad (4)$$

where $F_{max} = \alpha\eta H_{max}$ is the maximal motile force corresponding to the most convex cell shape, with curvature $H_{max} = 1/R$, where $R \simeq 10$ μm is the typical cell radius, F_0 is the baseline value for flat or concave cells, and $\alpha = (F_{max} - F_0)/H_{max}\eta$ is the proportionality ratio between the curvature and the cellular forces. Note that there is an

asymmetry to the cellular motion, such that cells at the edge always produce an outwards-directed force, toward the free substrate. Comparing our simulations to the experiments (see, for example, Fig. 3), we conclude that $F_0 << F_{\max}$, in a culture that is not activated by growth-factors. To simplify our analysis we therefore take $F_0 = 0$ for the rest of this article, although it probably does have some small nonzero value. When the cell culture is activated by growth-factors (3,18), F_0 can become comparable to $F_{\max}$, and the effect of the curvature is abolished (Fig. 1 *b*), and indeed the formation of fingers is suppressed (3).

Cells have the ability to remodel their cytoskeleton so that they can accommodate some changes in their projected area without resisting elastically, if stretched/compressed over long timescales compared to the timescales of cytoskeleton reorganization (typically of approximately tens of minutes). We treat here the cell area in an averaging manner, by averaging over the entire surface area of the cell culture. This means that we do not describe variations in the cell density within the culture (as observed in (6)). As long as the average cell area is smaller (larger) than some upper (lower) limit, there is, therefore, no elastic restoring force. Beyond these limits there is an elastic restoring force, which we assume here for simplicity to be linear. Note that only the stretching restoring force is reached in our simulations. Below a minimal average cell density $\rho_{\min}$, the cells cannot tolerate the stretch, and F_ρ becomes negative (restoring). In other words, the cells are assumed to have a maximal average area per cell $1/\rho_{\min}$, and a larger area (lower density), leads to stretching of the cells that give rise to an elastic linear restoring force. The same relation holds similarly for compression above a maximal density threshold, $\rho_{\max}$. The bulk restoring force due to the average cell density F_ρ is taken to have the form

$$F_\rho = \begin{cases} -\kappa_\rho\left(\frac{1}{\rho}-\frac{1}{\rho_{\min}}\right) & \rho < \rho_{\min} \\ 0 & \rho_{\max} > \rho > \rho_{\min} \\ -\kappa_\rho\left(\frac{1}{\rho}-\frac{1}{\rho_{\max}}\right) & \rho > \rho_{\max} \end{cases}, \quad (5)$$

where κ_ρ is the effective modulus of cell stretching. As long as the average cell density (ρ) is larger than the minimal density ($\rho_{\min}$) this force is zero, even if the density falls below the target density of the cells at the initial time (ρ_0).

Using F_{cell} as defined in Eq. 4, and applying it in Eq. 3, we get

$$\frac{d\vec{r}}{dt} = -\frac{\kappa}{\eta}\frac{\partial^4\vec{r}}{\partial s^4} + \sigma(H)\frac{\partial^2\vec{r}}{\partial s^2} + v_{\max}\theta(-H_{\max}-H)\hat{n} - \frac{3\kappa}{2\eta}\left|\frac{\partial^2\vec{r}}{\partial s^2}\right|^2\frac{\partial^2\vec{r}}{\partial s^2} + \frac{F_\rho}{\eta}\hat{n} + v\hat{n}, \quad (6)$$

where θ is the Heaviside step function and $v_{\max} = F_{\max}/\eta$. The active tension modulus σ is given by

$$\sigma = \begin{cases} \frac{\gamma}{\eta} - \alpha & 0 < -H < -H_{\max} \\ \frac{\gamma}{\eta} & \text{elsewhere} \end{cases}. \quad (7)$$

This coefficient becomes negative in some range of curvatures, i.e., inducing a shape instability. The curvature term eventually dominates at large curvatures, stabilizing the growth on small length-scales. Note that without the bending term in Eq. 6, whereby the surface tension is the only shape-dependent force, the fingers grow into singular cusps, which is not what is observed in the experiment (3,4).

Linear stability analysis

The interplay between the restoring forces and the curvature-induced motility drives a dynamic instability, as we now demonstrate using a linear stability analysis of our model. This linearized version (*dashed line* in Fig. 1 *b*) is valid in the regime of small perturbations from the flat interface, which exists at the beginning of the growth. In this limit the contour is almost perfectly aligned along the x axis, and the height undulations along the y axis of the contour coordinate are denoted by h (Monge gauge, Fig. 1 *a*). Equation 6 for the contour coordinate $\vec{r}(s)$ becomes an equation for the contour height along the x axis, i.e.: $h = \vec{r}\cdot\hat{y}$ and $s \to x$,

$$\frac{\partial h}{\partial t} = -\frac{\kappa}{\eta}\frac{\partial^4 h}{\partial x^4} - \left(\alpha - \frac{\gamma}{\eta}\right)\frac{\partial^2 h}{\partial x^2}. \quad (8)$$

A mode analysis of this equation, using $h(q) = h_0 \exp[\omega(q)t]$, where q is the wavenumber, and $\omega(q) = -\kappa q^4/\eta + (\alpha - \gamma/\eta)q^2$ is the dispersion relation (Fig. 1 *c*), indicates that an instability ($\omega(q) > 0$) occurs for wavenumbers $q < q_c$, given by

$$q_c = \sqrt{\frac{\alpha\eta - \gamma}{\kappa}}. \quad (9)$$

The wavenumber with the maximal positive ω is $q_{\max}$, given by $q_{\max} = q_c/\sqrt{2}$, and is the initial wavelength of the fingers that spontaneously form at the beginning of the interface evolution, according to our model. Note that, to perform the linear analysis, we have to replace F_{cell} of Eq. 4 with some approximate analytic expression at $\sim H = 0$. As a consequence, the actual slope near the zero curvature point is somewhat smaller than α, which results in a smaller $q_{\max}$ and a wavelength that is larger than the most unstable wavelength we wrote above (Fig. 1 *b*).

Beyond the initial stages of the growth, we need to simulate numerically the evolution of the interface, using Eq. 6. In this calculation scheme the coordinate $\vec{r}$ is represented as a function of s, and we calculate the spatial and temporal derivatives using the Euler method. To keep a certain resolution in the spatial discretization of the contour, and therefore maintain the stability of the numerical calculation without reducing the integration time step, we redistribute the grid

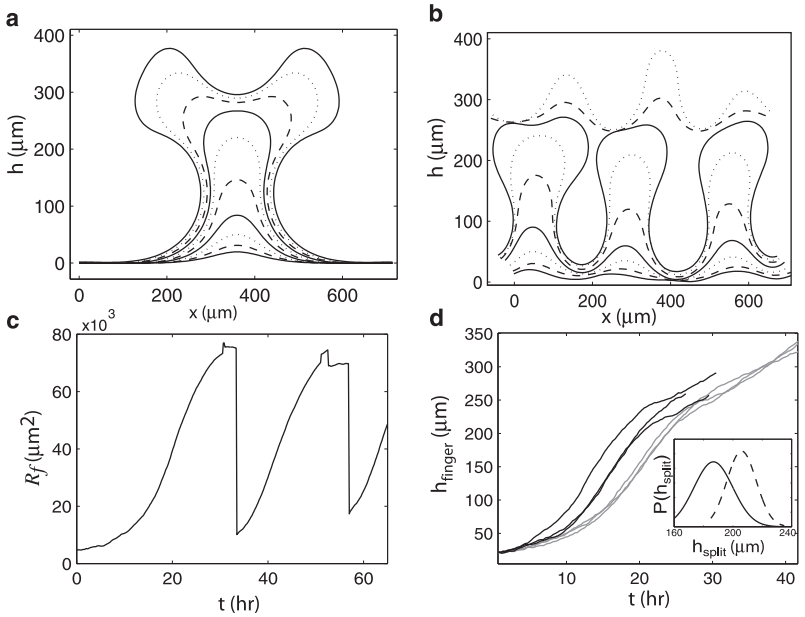

FIGURE 2 (*a*) Deterministic evolution ($\nu = 0$) of the contour from an initial Gaussian perturbation of height 1 μm, at different times (each contour is 5 h apart), using $\beta = 0.1$. (*b*) Using the same parameters as in panel *a* but with random cellular noise ν, at times 5–40 h (each contour is 5 h apart). (*c*) Roughening cycles of the contour from simulation in panel *b*. (*d*) Fingers split at the same range of heights, for both tensions $\beta = 0.1, 0.2$ (*solid* and *shaded lines*, respectively). The different lines give different realizations of the random noise. (*Inset*) Absolute location of the tip-splitting for $\beta = 0.1, 0.2$ (*solid* and *dashed lines*, respectively).

points during the calculation, either by adding or removing points or by equally redistributing the grid points along the contour. After tip-splitting of the growing fingers (Fig. 2, *a* and *b*, and Fig. 3), two different fingers collide. In the simulation we join the contour at the collision point, removing the grid points in between (Fig. 2 *b* and Fig. 3). In the experiments the fingers merge and the hole that is created closes with time as cells move in to fill the empty substrate, in a purse-string fashion (1).

Quantities of the parameters in the model

We now give the quantitative values that we estimated for the different parameters used in our simulations. We start with estimating the maximal value of the motile force that the cells can produce, $F_{\max}$ (Fig. 1 *b*). For this estimate we use the order of magnitude of the maximal observed velocity of independent motile cells, $v_{\max} \sim 70$ μm/h (as seen in some of our experiments for detached cells and as reported in (37,38)), because this maximal velocity arises from the maximal motile forces that these cells can produce when they are not held back by the continuous culture (cell-cell contacts). Indeed the actual maximal velocity of the cells when part of the continuous culture is much lower (see Fig. 6). Using this estimation for the maximal value of the motile velocity of these cells, we fix the curvature-induced force (Eq. 4), $\alpha = v_{\max}/H_{\max}$ (we take $H_{\max} = 0.1$ μm^{-1}). The effective surface tension, γ, is a free parameter that we denote in proportion to α, such that $\gamma/\eta = \beta\alpha$. We next fix the value for the average initial separation between fingers, $\lambda = 2\pi/q_{\max}$, to be ~180 μm. Using Eq. 9 we can then find the value of the combination κ/η, as $\kappa/\eta = \alpha(1-\beta)/2q_{\max}^2$. Finally, the magnitude of the random cellular velocity ν (noise term) is taken from the experimental distribution which is fitted to a Gaussian (unpublished data), with a zero mean and standard deviation of 5 μm/h. This noise term is drawn from the random Gaussian distribution every 20 min, which is the typical persistence time for cellular motility observed in different cell types (18,39). Note that the actual distribution of traction forces seems to have an exponential form (6), but this detail is not crucial for our purposes. We further smooth this noise term over the grid points along the length of a cell diameter (2R), such that the random velocity changes over this cellular length-scale. Finally, for the elastic restoring force due to low cell density, we used the value $\kappa_p/\eta = 4.4 \times 10^{-4}$ (μm s)$^{-1}$, which is of the order of magnitude found in experiments on cell stretching (40).

RESULTS

We now present the results of the simulations of the evolution of the culture contour, according to our model presented in Eq. 6. We start by neglecting the bulk restoring force due to overall cell stretching, by putting $F_\rho = 0$ in Eq. 6. The results of a deterministic evolution (no noise $\nu = 0$) is shown in Fig. 2 *a*, where we start with an initial Gaussian shape perturbation, of amplitude 1 μm. We see that the main perturbation grows and begins to split at the tip, when the amplitude reaches a height that is ~λ. A similar growth, and splitting of fingers occur when we start with a flat contour, but include the random noise in the cell velocity (Fig. 2 *b*), which is shown to be enough to trigger the instability. The fingers grow at an initial separation of λ, but at later times coalesce to form fewer but larger fingers, due to nonlinear dynamics. Whenever the contour collides with itself, we employ a joining algorithm, and recover the shape of the outer contour. This type of dynamics gives rise to cycles of

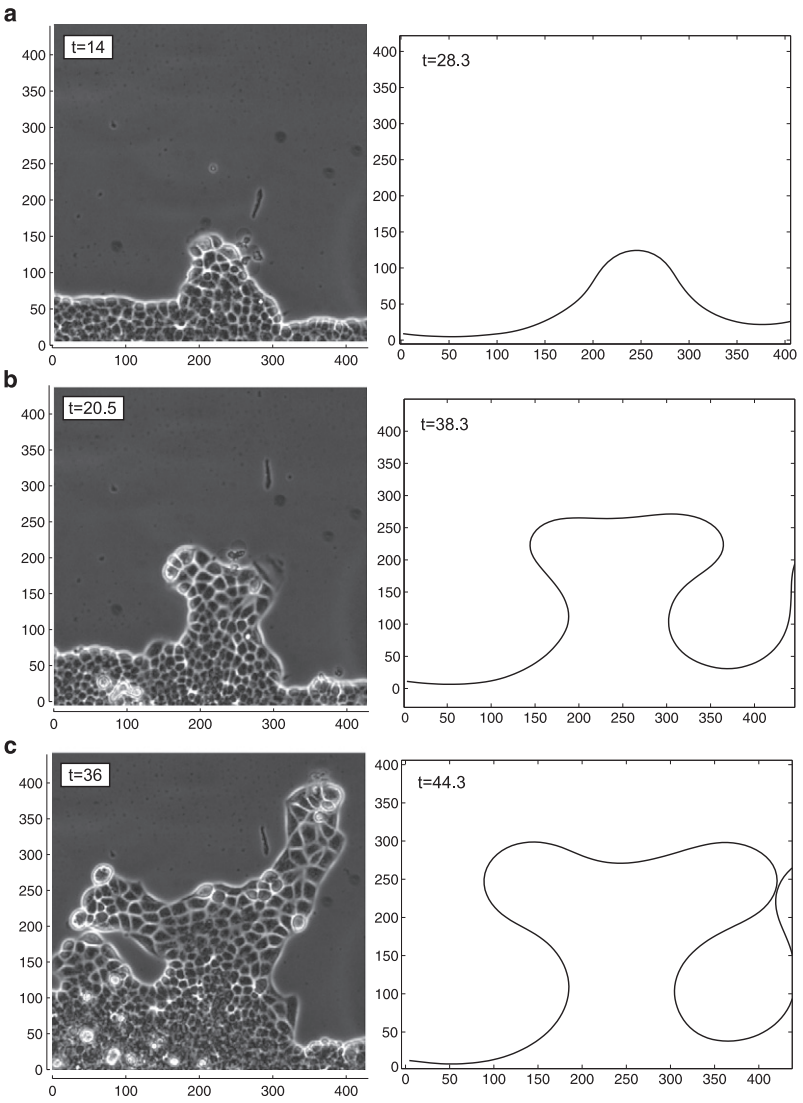

FIGURE 3 Qualitative comparison between the calculated evolution of the fingers (*right*) and the experiment (*left*). Lengths are in μm, and the times are in hours. The simulations were done using $\beta = 0.1$.

roughening and smoothing of the moving contour, as shown in Fig. 2 *c*. Note that the joining algorithm gives rise to large discontinuous drops in the roughness parameter ($R_f = \langle (h - \langle h \rangle)^2 \rangle$), whenever we remove a loop of closed contour. Note that at the joining site, we remove and smooth-out the cusp formed by the two contour parts.

The height of the fingers at which they begin to split, is determined by the same length-scale λ, as we demonstrate in Fig. 2 *d*. Here we plot the mean finger height $h_{\text{finger}} = h_{\max} - h_{\min}$ for two different contour tensions, and for several realizations of the noise (where $h_{\max}$ is the height of the finger tip, and $h_{\min}$ is the value at the finger base). In both cases we kept the value of $\lambda \sim 180$ μm fixed, by adjusting the value of η accordingly, so that the average finger height at the splitting is the same in both cases. When the tension is large, the contour moves together in a more uniform manner, and the time it takes for the undulations (fingers) to reach an amplitude of $\sim\lambda$ and split is similarly larger. The velocity of the fingers is further reduced by the increase in the restoring force (Fig. 2 *d*), and the splitting events therefore occur at a larger mean displacement with respect to the initial culture boundary (Fig. 2 *d*, *inset*). Fingers in the experiments indeed show a variety of lengths before they split (or bulge). We interpret this observation as indicative of the large local variations in cellular motility and strength of cell-cell adhesion, which determines the local values of the effective bending modulus and tension.

In Fig. 3 we show a qualitative comparison between one simulation result with a particular evolution of a single finger in the experiment (experimental details are given in the Supporting Material). We see in this figure the stages of the evolution of a finger as it grows, splits, and merges. We see that indeed in the experiment the internal closed-contour fills with cells behind the main front. Whereas events of finger splitting and merging always occur in the fingers of the simulations, they appear much less often in the experiments, where tip bulging is observed. This indicates the shortcomings of the continuum model that does not properly describe the discrete

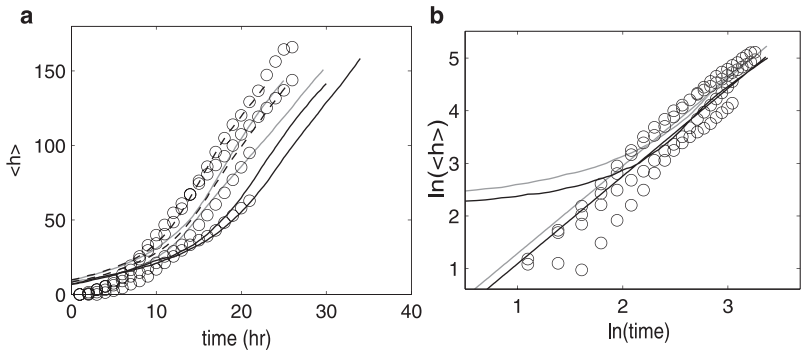

FIGURE 4 (*a*) Evolution of the increase in the mean width of the expanding cell culture. Measurements for a rectangular culture of initial width 200 μm are given in circles. Solid lines are the results of our simulations for different realizations of the cellular noise, and different surface tension: $\beta = 0.05$, 0.1, 0.2 (*dashed*, *shaded*, and *solid lines*, respectively). (*b*) A log-log plot of the data in panel *a*. The solid lines are two simulations, and the straight lines are fits to a power-law behavior, with slopes of 1.7.

cellular behaviors at the tips of the fingers, where there is sometimes just a single leader cell. In Fig. 3 *c*, the finger in the experiment is observed to go through a second tip-splitting event, which in the simulations is also observed if there is enough space for this to occur before fingers merge (see Fig. 7 *a* for an example). Future detailed experiments may provide quantitative statistics regarding the tip-splitting events, so that detailed comparisons of this phenomenon can be made to the model.

We now make quantitative comparisons between our model and the observed evolution of the culture contour. The growth of the mean width of the rectangular culture (Fig. 1 *a*), which is simply the average of the height coordinate $\langle h \rangle$ as a function of time, is shown in Fig. 4 *a*, up to the first contour-join event. We find that the calculated mean culture width increases in an accelerating manner, after some incubation period. This acceleration occurs in our model due to the instability mechanism whereby the fingertips increase their velocity as they grow and become more curved (Eq. 4). This behavior is more clearly seen in the log-log plot (Fig. 4 *b*). Note that the definition of the initiation time of the fingers ($t = 0$) is somewhat arbitrary and difficult to define clearly. The fingers seem to develop more quickly in the experiments as compared to the simulations and this is most likely due to the continuum nature of our model, which ignores the discrete nature of the cells, i.e., the leader cell acts as a single unit whereas in our model there is a continuum velocity field along the contour.

By fitting the growth to a power-law (for $t > 7.5$ h) we demonstrate that the growth has an approximately quadratic behavior during a certain period, as found in the experiment (3) (the value of the power is not exactly 2). In both the simulations and the experiments the growth becomes linear after the acceleration period, so that the overall agreement between the observations and the model is good. The spread in the observed culture width growth is also captured by the model, indicating that it originates from the noise in the motion of the individual cells. Increasing the surface tension, while keeping the value of the most unstable wave-length constant (therefore the parameter κ/η is adjusted), decreases the growth rate of the mean culture width (Fig. 4 *a*), due to the larger restoring force.

We next add the restoring force due to cell stretching as a result of the reduction in average cellular density in the expanding culture. We will make use of the observations that the number of cells increases roughly linearly with time in these cell cultures. The number of cells as a function of time is therefore written as $N = N_0(1 + \zeta t)$, which results in a mean cellular density given by $\rho = \rho_0(1 + \zeta t)/(1 + 2\langle h \rangle(t)/w)$ (where the mean culture width increases in both directions for a rectangular island of cells of initial width w; see Fig. 1 *a*). Note that we consider that cell proliferation is triggered by the release of the confinement, which we chose to be the time that the contour has moved by approximately a cell's length of 10 μm. When ρ reaches a maximal value (which we take to be $\rho_{\max} \sim 5.7 \times 10^{-3}$ cells/μm^2), the cell proliferation stops due to cell-cell migration contact inhibition (17). Note that, in the real culture, there is no such sharp transition to zero proliferation above a threshold density, but instead a gradual decrease in the overall proliferation rate. In Fig. 5 *a*, we plot the evolution of the average cellular density for cultures of several initial widths, where we calibrated the value of ζ from the observed linear increase at small times for a 200-μm strip (Fig. 5 *a*). At the beginning, the culture expansion velocity is low, and therefore the density of cells increases. Later, when the fingers start to grow, the culture area grows faster than linearly with time and as a consequence the average cell density decreases (our calculations are limited to times before the first contour-join events; see Fig. S1).

When the average cell density falls below $\rho_{\min} = (4/5)\rho_0$ (arbitrarily chosen; note that this is the average value over the whole culture, whereas cells at the culture front are observed to have an area that is up to 2–3 times that of cells further behind), the additional elastic restoring force F_ρ (Eq. 5) leads to a much reduced rate of culture expansion (Fig. 5 *b*). Because the initial width of the rectangular culture is smaller the restoring effect of the cell stretching on the culture expansion appears earlier, as the culture reaches the minimal density $\rho_{\min}$ at an earlier time. Decreasing the proliferation rate to zero ($\zeta = 0$) leads to a similar behavior, whereby the culture expansion proceeds normally for relatively short times ($t < 10$ h) as observed in the experiments (3), but slows down eventually when the density falls below $\rho_{\min}$ (Fig. 5 *a*).

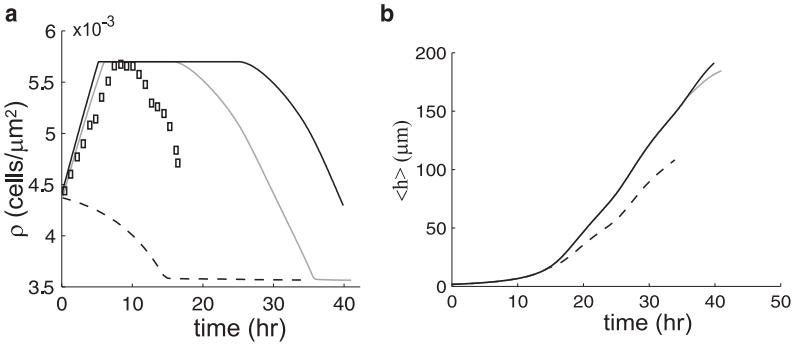

FIGURE 5 (*a*) Calculated average cell density ρ as a function of time, for a 200-μm and 100-μm initial culture-width (*solid* and *shaded lines*), compared to the observed data (*squares*). The case of no proliferation is given by the dashed line. (*b*) The corresponding growth of the mean culture-width, corresponding to the cases shown in panel *a*.

By following the dynamics of the leader cells, i.e., the tips of the growing fingers, we can compare our calculations to the observed behavior, shown in Fig. 6. In Fig. 6 *a*, we plot the observed and simulated evolution of the tips of several fingers $h_{\max}(t)$, as a function of time. The simulations are in good agreement with the observations; we see that in both the experiment and the calculation the velocity of the tip (leader cell) v_{tip} goes through periods of acceleration and slowing down (Fig. 6 *a*). These variations in the tip velocity are correlated in the simulations with the changes to the tip curvature H_{tip} when the tip of the finger flattens and splits (Fig. 6, *b* and *c*). The leader cells in the experiments also experience decelerations (~12.5, 12, and 20 h for the *dashed*, *shaded*, and *solid traces*, respectively), although these variations around the mean velocity of the leaders were observed to be small. The discrete nature of the leader cells suppresses full tip-splitting events compared to the continuum simulations, but the mechanism that leads to the slowing-down of the leader cells is still the same; they consistently showed a slowing-down related to the bulging (flattening) of the tip. Similarly, the continuum simulations describe a slower rise of the tip velocity compared to the observations, where the leader cells attain their final velocity faster.

It can be seen that increasing the effective surface tension (cell-cell contacts) decreases the growth rate of the maximal height of the fingers. The maximal velocity of the leader cells that we calculate (~18 μm/h) is much lower than $v_{\max}$ due to the restoring force of curvature of the culture front. Note that this agreement is a nice check of the consistency of the chosen parameters, which were fixed to reproduce the initiation spacing of the fingers.

DISCUSSION AND CONCLUSIONS

A growing cell culture is a complex process that is affected by diverse factors such as chemical and mechanical signaling (12,15). Most of the research done in the context of collective growth and migration focuses on diffusing chemicals as the major guide, with or without mechanical cues of various forms. In this work we excluded all these effects and focused on the influence of the shape of the culture as the only mechanical cue that guides this process. We have shown that this component alone can induce in an expanding culture behavior similar to that seen in experiments (3): The culture interface in this model can become unstable; columns of cells (fingers) form and grow with time. Furthermore, we show that the bending restoring force of the cells gives rise to the phenomenon of tip-splitting. The bending energy is crucial to this type of instability, as otherwise the fingers grow into a singular cusp, which is not what is observed in the experiment (3,4). As long as the effective surface tension of the culture interface is not larger than the slope of the curvature-velocity rule (Eq. 4), there are unstable wavelengths. The value of the effective surface tension simply affects the values of the mean growth velocity and the height of fingers at which tip-splitting occurs, but qualitatively the same shapes and behavior can be seen without surface tension at all.

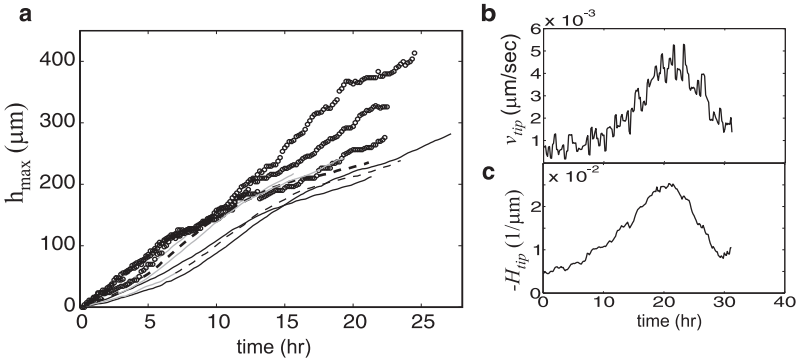

FIGURE 6 (*a*) Evolution of the position of fingertips; points, experimental observations of leader cells (3), lines, using our model for different tensions ($\beta = 0.05$, 0.1,and 0.2, *shaded*, *dashed*, and *solid lines*, respectively). (*b* and *c*) Evolution of the tip velocity and curvature for the finger shown in the dashed line in panel *a*. Note that the initial time $t = 0$ is shifted in panel *a* to compare to the experimental data, which begins only when the finger is distinguishable for the first time.

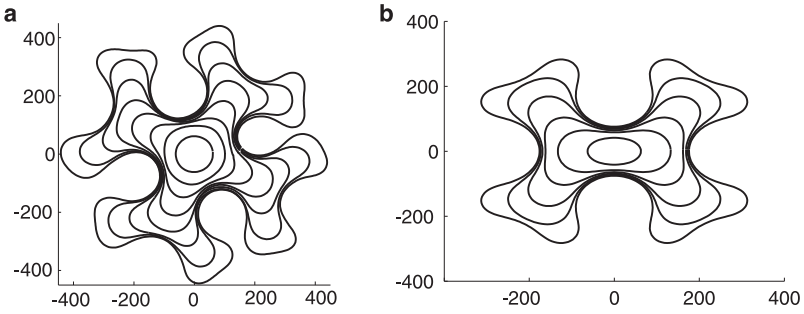

FIGURE 7 (*a*) Calculated expansion of an initially circular culture, in the presence of cellular noise. (*b*) An initially elliptic culture expands and develops fingers even in the absence of noise. In both plots the time between contours is 5 h, and the lengths are in μm.

Our model allows us to make a number of testable and quantitative predictions. We predict:

1. that the contour of an expanding culture should go through roughening/smoothing cycles (Fig. 2 *d*);
2. that the rate of cell proliferation determines the time at which the culture expansion slows down; and
3. that the average distance between fingers should depend on the effective elastic moduli of the cells (γ and κ) as well as on the slope of the curvature-velocity rule (α, Eq. 4).

The elastic moduli of the culture interface may be modified through the strength of the cell-cell adhesion contacts, as well as the elasticity of the individual cells. The slope α can be changed by modifying the overall motility of the cells. For example, increasing F_0 from zero to some finite value smaller then F_{max} (without changing F_{max}) decreases the slope α (Fig. 1 *b*) and q_c (Eq. 9), and increases the most unstable wave length, λ. If λ is larger than the length of the culture, no fingering will form. This prediction may explain the observed absence of fingers when growth-factor was added to the medium (3,18); within our model the effective value of F_0 may increase in response to the growth-factors. The growth-factors most likely also modify the cell-cell adhesions, cell motility, and therefore the effective elastic parameters γ, κ of our contour. Due to the faster motility in the presence of growth-factors (23,41), the interface will expand faster, whereas fingers with larger λ take a longer time to develop. A similar change in the average separation of fingers is shown in Fig. S3 of Trepat et al. (6) as a function of the substrate rigidity, which modifies the adhesiveness of the cells and therefore their traction forces F_{max}.

Different culture geometries can be used to test the model, such as a circular and an elliptical shape. For a perimeter that is larger than the minimal unstable wavelength, the expanding circular interface develops fingers (Fig. 7 *a*). A contour with an initial elliptic shape grows faster along the major axis, where the curvature is higher, and therefore elongates with time (Fig. 7 *b*). In both of these examples, we neglected the effects of bulk cell stretching ($F_\rho = 0$).

To conclude, we have shown that the shape of a culture interface can play an important role in collective cell migration during wound healing, and may play an important role in other phenomena such as morphogenesis (34,42). We suggest that a future model, which integrates the culture shape with the chemical and mechanical signaling, may lead to a better description of these collective cellular phenomena.

SUPPORTING MATERIAL

One figure is available at http://www.biophysj.org/biophysj/supplemental/S0006-3495(09)01629-4.

P.S. gratefully acknowledges financial support from the Association pour la Recherche sur le Cancer. N.S.G. thanks the Alvin and Gertrude Levine Career Development Chair for its support. This research was partially supported by the Israel Science Foundation (grant No. 337/05). This research is also made possible in part by the historic generosity of the Harold Perlman Family.

REFERENCES

1. Jacinto, A., A. Martinez-Arias, and P. Martin. 2001. Mechanisms of epithelial fusion and repair. *Nat. Cell Biol.* 3:E117–E123.
2. Farooqui, R., and G. Fenteany. 2005. Multiple rows of cells behind an epithelial wound edge extend cryptic lamellipodia to collectively drive cell-sheet movement. *J. Cell Sci.* 118:51–63.
3. Poujade, M., E. Grasland-Mongrain, …, P. Silberzan. 2007. Collective migration of an epithelial monolayer in response to a model wound. *Proc. Natl. Acad. Sci. USA.* 104:15988–15993.
4. Nikolić, D. L., A. N. Boettiger, …, S. Y. Shvartsman. 2006. Role of boundary conditions in an experimental model of epithelial wound healing. *Am. J. Physiol. Cell Physiol.* 291:68–75.
5. Haga, H., C. Irahara, …, K. Kawabata. 2005. Collective movement of epithelial cells on a collagen gel substrate. *Biophys. J.* 88:2250–2256.
6. Trepat, X., M. R. Wasserman, …, J. J. Fredberg. 2009. Physical forces during collective cell migration. *Nat. Phys.* 5:426–430.
7. Martin, P., and S. M. Parkhurst. 2004. Parallels between tissue repair and embryo morphogenesis. *Development.* 131:3021–3034.
8. Parent, C. A., and P. N. Devreotes. 1999. A cell's sense of direction. *Science.* 284:765–770.
9. Lauffenburger, D. A., and A. F. Horwitz. 1996. Cell migration: a physically integrated molecular process. *Cell.* 84:359–369.
10. Yin, J., K. Xu, …, F. S. Yu. 2007. Wound-induced ATP release and EGF receptor activation in epithelial cells. *J. Cell Sci.* 120:815–825.
11. Gov, N. S. 2007. Collective cell migration patterns: follow the leader. *Proc. Natl. Acad. Sci. USA.* 104:15970–15971.
12. Sherratt, J. A., and J. D. Murray. 1991. Mathematical analysis of a basic model for epidermal wound healing. *J. Math. Biol.* 29:389–404.
13. Dale, P. D., P. K. Maini, and J. A. Sherratt. 1994. Mathematical modeling of corneal epithelial wound healing. *Math. Biosci.* 124: 127–147.

14. Cai, A. Q., K. A. Landman, and B. D. Hughes. 2007. Multi-scale modeling of a wound-healing cell migration assay. *J. Theor. Biol.* 245:576–594.

15. Fenteany, G., P. A. Janmey, and T. P. Stossel. 2000. Signaling pathways and cell mechanics involved in wound closure by epithelial cell sheets. *Curr. Biol.* 10:831–838.

16. Rosen, P., and D. S. Misfeldt. 1980. Cell density determines epithelial migration in culture. *Proc. Natl. Acad. Sci. USA.* 77:4760–4763.

17. Shraiman, B. I. 2005. Mechanical feedback as a possible regulator of tissue growth. *Proc. Natl. Acad. Sci. USA.* 102:3318–3323.

18. Bindschadler, M., and J. L. McGrath. 2007. Sheet migration by wounded monolayers as an emergent property of single-cell dynamics. *J. Cell Sci.* 120:876–884.

19. Walker, D. C., G. Hill, …, J. Southgate. 2004. Agent-based computational modeling of wounded epithelial cell monolayers. *IEEE Trans. Nanobioscience.* 3:153–163.

20. Ouaknin, G. Y., and P. Z. Bar-Yoseph. 2009. Stochastic collective movement of cells and fingering morphology: no maverick cells. *Biophys. J.* 97:1811–1821.

21. Gov, N. S. 2009. Traction forces during collective cell motion. *HFSP J.* 3:223–227.

22. Reference deleted in proof.

23. du Roure, O., A. Saez, …, B. Ladoux. 2005. Force mapping in epithelial cell migration. *Proc. Natl. Acad. Sci. USA.* 102:2390–2395.

24. Brock, A., E. Chang, …, D. E. Ingber. 2003. Geometric determinants of directional cell motility revealed using microcontact printing. *Langmuir.* 19:1611–1617.

25. Parker, K. K., A. L. Brock, …, D. E. Ingber. 2002. Directional control of lamellipodia extension by constraining cell shape and orienting cell tractional forces. *FASEB J.* 16:1195–1204.

26. Verkhovsky, A. B., T. M. Svitkina, and G. G. Borisy. 1999. Self-polarization and directional motility of cytoplasm. *Curr. Biol.* 9:11–20.

27. Jiang, X., D. A. Bruzewicz, …, G. M. Whitesides. 2005. Directing cell migration with asymmetric micropatterns. *Proc. Natl. Acad. Sci. USA.* 102:975–978.

28. Cross, M. C., and P. C. Hohenberg. 1993. Pattern formation outside of equilibrium. *Rev. Mod. Phys.* 65:851–1112.

29. Langer, J. S. 1989. Dendrites, viscous fingers, and the theory of pattern formation. *Science.* 243:1150–1156.

30. Ben-Jacob, E. 1997. From snowflake formation to growth of bacterial colonies. *Contemp. Phys.* 38:205–241.

31. Bensimon, D. 1986. Stability of viscous fingering. *Phys. Rev. A.* 33:1302–1308.

32. Brower, R. C., D. A. Kessler, …, H. Levine. 1984. Geometrical models of interface evolution. I. *Phys. Rev. A.* 29:1335–1342.

33. Brower, R. C., D. A. Kessler, …, H. Levine. 1984. Geometrical models of interface evolution. II. *Phys. Rev. A.* 30:3161–3174.

34. Lubkin, S. R., and J. D. Murray. 1995. A mechanism for early branching in lung morphogenesis. *J. Math. Biol.* 34:77–94.

35. Bement, W. M., P. Forscher, and M. S. Mooseker. 1993. A novel cytoskeletal structure involved in purse-string wound closure and cell polarity maintenance. *J. Cell Biol.* 121:565–578.

36. Safran, S. A. 2003. Statistical Thermodynamics of Surfaces, Interfaces, and Membrane. Westview Press, Boulder, CO.

37. Dieterich, P., R. Klages, …, A. Schwab. 2008. Anomalous dynamics of cell migration. *Proc. Natl. Acad. Sci. USA.* 105:459–463.

38. Thurner, S., N. Wick, …, L. Huber. 2003. Anomalous diffusion on dynamical networks: a model for interacting epithelial cell migration. *Physica A.* 320:475–484.

39. Huang, S., C. P. Brangwynne, …, D. E. Ingber. 2005. Symmetry-breaking in mammalian cell cohort migration during tissue pattern formation: role of random-walk persistence. *Cell Motil. Cytoskeleton.* 61:201–213.

40. Gavara, N., P. Roca-Cusachs, …, D. Navajas. 2008. Mapping cell-matrix stresses during stretch reveals inelastic reorganization of the cytoskeleton. *Biophys. J.* 95:464–471.

41. Li, Y., M. M. Bhargava, …, I. D. Goldberg. 1994. Effect of hepatocyte growth factor/scatter factor and other growth factors on motility and morphology of non-tumorigenic and tumor cells. *In Vitro Cell. Dev. Biol.* 30A:105–110.

42. Moore, K. A., T. Polte, …, D. E. Ingber. 2005. Control of basement membrane remodeling and epithelial branching morphogenesis in embryonic lung by Rho and cytoskeletal tension. *Dev. Dyn.* 232: 268–281.